EUROPEAN COMMISSION
Community Research

SEVENTH FRAMEWORK PROGRAMME

CARBOWASTE

Treatment and Disposal of Irradiated Graphite and Other Carbonaceous Waste

Grant Agreement Number: FP7-211333

Deliverable (T-4.1.2)

Interim report on the relationships between structure and isotope distribution in graphite

Author(s): Abbie Jones; Greg Black; Lorraine McDermott

University of Manchester,

Werner von Lensa, Dirk Vulpius;
Forschungszentrum Juelich GmbH

Reporting period: e.g. 01/04/2008– 01/04/2010

Date of issue of this Report: 01/07/2010

Start date of project : **01/04/2008** Duration : **48 Months**

Distribution list

Person and organisation name and/or group	Comments
Task 4.1 members	
Executive Board	
Co-ordinator	

CARBOWASTE		
Work package: 4 **Task: :** 4.1.2 (and 4.11)	**CARBOWASTE document no:** CARBOWASTE-1002-D-wp4.Task.4.1.2 (e.g. May 2008 as date of issue: 0805)	**Document type:** Deliverable
Issued by: UoM **Internal no.:** UoM_WP3_D4.1.2 _Final		**Document status:** Final

Project co-funded by the European Commission under the Seventh Framework Programme (2007 to 2011) of the European Atomic Energy Community (EURATOM) for nuclear research and training		
Dissemination Level		
PU	Public	
RE	Restricted to the partners of the CARBOWASTE project	**X**
CO	Confidential, only for specific distribution list defined on this document	

Document title
Interim report on the relationships between structure and isotope distribution in graphite

Executive summary

This report will build on analysis of data for the various grades of unirradiated and irradiated graphite obtained in WP3 in conjunction with data obtained for the treated graphite in WP4. This combines tasks 4.1.1 (Indicative relationships between structure and isotope distribution in graphite) and 4.1.2 (Interim report on the relationships between structure and isotope distribution in graphite) for the Deliverable.

Mechanistic background of impurity / isotope localisation before and after treatment is required to feed into the treatment options within WP4 and subsequent work packages. A literature review is underway to investigate the mechanistic background of impurity content and removal of irradiated graphite waste. The process involved in predicting the end of life radionuclide inventory has been identified and research is underway in order to apply this to a statistical model for impurity removal. Techniques such as ICPGC-MS, Autoradiography, SEM-EDX and X-ray tomography have also been highlighted for the analysis of impurity and isotopic location within the graphite. These models for the removal of the contaminants will be defined and validated against the data and known inventories and will be developed over the next two years. A fundamental understanding radionuclide origins, location as removal mechanisms, combined with the development of improved graphite purification methods, may enable the manufacture of new grades of nuclear graphite with lower impurity concentrations being important for both, improved neutronics and waste minimisation.

Revisions

Rev.	Date	Short description	Author	Internal Review	Task Leader	WP Leader

00	01/04/2010	Issue	AN Jones UoM	von Lensa FZJ	ANJ UoM	von Lensa FZJ
01	01/07/2010	First issue	AN Jones UoM	von Lensa FZJ	ANJ UoM	von Lensa FZJ

Table of Contents

1 Introduction

The radionuclide content of irradiated graphite from nuclear reactor cores can arise from two sources: intrinsic and extrinsic. Intrinsic radioactivity results from the neutron activation of Carbon and other stable impurities within the graphite structure; these impurities are residue from the manufacturing process [1]. Extrinsic radioactivity is the result of surface contamination from other components in the reactor circuit due to damage and corrosion; possible sources include fuel cladding, pressure vessel, coolant gas and various other support structures [2]. In some cases this contribution can be relatively large, as for AGRs which have been contaminated with cobalt containing metal oxides within the reactor circuit leading to a significant further Co-60 contribution [2]. An additional source of radioactivity, which may be of either an intrinsic or extrinsic origin, are fission products which will arise from both the fuel and the natural Uranium impurity of the graphite (below 0.1ppm [2, 3]) when undergoing fission [2]. The origin of the radionuclides will therefore determine the location; an extrinsic origin will give rise to surface bound adsorped radionuclides whereas an intrinsic origin will result in the radionuclide being 'trapped' either interstially or intercalated in inside the graphite structure.

It may be possible, through the application of various treatment techniques [4-6] to remove the surface radionuclides without compromising the structural integrity of the graphite components, however any radionuclides which are located within the graphite structure will only be removed through the application of destructive techniques [7]. Thus the quantification of the impurity content of the graphite is an important factor in determining not only the end of life radioactivity of the graphite as well as the location, and therefore, the necessary treatment regime required to remove these.

1.1 Origin of impurities

The manufacturing process for nuclear grade graphite may include supplementary baking and reimpregnation steps [1, 8] to ensure the purity of the material it is impossible to remove all the impurity content, in addition the process itself will also result in the introduction of impurity elements such a Cl gas [1]. Accurate information regarding the impurity inventory of nuclear graphite grades is limited, however various studies have shown that impurities levels are relatively low and measured in parts-per-million (ppm) [3]. One such study was performed by White et al, 1984[3], which experimental determined the impurity content of the graphite grades used in the UK Magnox and AGR class of reactors; the results of which are detailed in Table 1.

Table 1: Reference Graphite impurity levels [3]

Element	Magnox (ppm)	AGR (ppm)	Element	Magnox (ppm)	AGR (ppm)
Li	0.05	0.05	Ni	1.0	6.0
Be	0.02	0.02	Zn	0.13	1.0
B	0.1	0.5	Sr	0.4	0.4
N	10	10	Mo	0.1	2.5
Na	1.0	4.0	Ag	0.001	0.001
Mg	0.1	0.4	Cd	0.04	0.07
Al	1.0	4.0	In	0.05	0.06
Si	35	35	Sn	0.05	1.0
S	50	60	Ba	1.5	0.5
Cl	2.0	4.0	Sm	0.04	0.05
Ca	35	25	Eu	0.004	0.005
Ti	3	0.7	Gd	0.005	0.01
V	12	0.4	Dy	0.008	0.006
Cr	0.35	0.4	W	0.12	0.15

Mn	0.04	0.25	Pb	0.12	0.8
Fe	10	28	Bi	0.08	0.05
Co	0.02	0.7	Ni	1.0	6.0

1.2 Activation Inventory Products

White et al (1984) then performed a simulation, using the United Kingdom Atomic Energy Agency (UKAEA) FISPIN© software (a nuclide inventory calculation code) to calculate the resultant radionuclides from the impurities in Table 1 after a reactor lifetime of 40 years followed by 10 years storage time. The calculated results for reference Magnox and AGR reactors are given in Table 2.

Table 2: Activation inventory for reference Magnox (2233tonnes of graphite) and AGR (1633tonnes of graphite) [from [2]]

Radionuclide	Magnox (Bq)	AGR (Bq)	Radionuclide	Magnox (Bq)	AGR (Bq)
H-3	1.2×10^{14}	7.6×10^{13}	Mo-93	8.5×10^{8}	8.5×10^{10}
Be-10	7.1×10^{10}	2.3×10^{11}	Nb-93m	5.5×10^{8}	3.4×10^{10}
C-14	8.5×10^{13}	1.9×10^{14}	Nb-94	1.0×10^{5}	8.4×10^{6}
Cl-36	9.5×10^{11}	2.3×10^{12}	Tc-99	1.7×10^{8}	5.6×10^{9}
Ca-41	7.3×10^{11}	1.2×10^{12}	Ag-108m	2.3×10^{10}	3.6×10^{10}
Mn-54	2.7×10^{8}	5.2×10^{9}	Cd-113m	1.0×10^{10}	4.4×10^{10}
Fe-56	1.5×10^{13}	9.3×10^{13}	Sn-121m	4.5×10^{10}	2.8×10^{12}
Ni-59	9.3×10^{10}	5.5×10^{11}	Ba-133	5.6×10^{11}	3.1×10^{11}
Co-60	2.7×10^{13}	9.8×10^{14}	Eu-152	2.2×10^{11}	1.0×10^{11}
Ni-63	1.3×10^{13}	1.1×10^{14}	Eu-154	2.2×10^{12}	2.9×10^{12}
Zn-65	2.1×10^{8}	3.7×10^{9}	Eu-155	1.6×10^{12}	9.4×10^{11}

From these activation products the beta emitting C-14 ($t_{1/2}$ = 5730 y), H-3 ($t_{1/2}$ = 12.32 y) and Cl-36 ($t_{1/2}$ = 301,000 y) isotopes are considered to represent the most likely contaminates to the food chain, and gamma emitting nuclides including Co-60 ($t_{1/2}$ = 5.2714 y), Nb-94 ($t_{1/2}$ = 20,300 y), Eu-152 ($t_{1/2}$ = 13.537 y) and Eu-154 ($t_{1/2}$ = 8.593 y) will complicate any dismantling, handling and storage requirements[2]. In order to quantify the final activity of individual radioisotopes it is important to consider the routes from which these are generated, for example Carbon-14 is produced by a variety of routes, the dominant ones identified as: $^{14}N(n,p)^{14}C$, $^{13}C(n,\gamma)^{14}C$ and $^{17}O(n,\alpha)^{14}C$. The contribution per route is related to both the reaction-cross section and also the quantity of the impurity available (both as a virgin impurity and from core contamination). Currently there is a debate within the scientific community to the significance of each production route and their contributions to final Carbon-14 content, it is hoped that work within the Carbowaste Wp4 program will provide an insight into these mechanisms and the dominance.

Tritium (H-3) also has a variety of production routes the main contribution estimated to be from neutron activation of the Li impurity, through the (n, p) reaction route [9, 10]with additional production pathways from Boron and Nitrogen (both present as impurities in the core). Chlorine-36 may arise from the activation of Chlorine impurities within the graphite which are present as a result of its use during purification of the graphite [11].

The contribution to the radionuclide inventory from the fission of uranium fuel and impurity was also calculated, the results are given in Table 3.

Table 3: Inventory (Bq) for irradiation of 0.1ppm natural Uranium in reference Magnox & AGR (40 years lifetime operation followed by 10 years decay) [from [2]]

Magnox				AGR			
Se-79	1.80×10^{6}	Eu-152	3.19×10^{7}	Se-79	2.98×10^{6}	Eu-152	2.53×10^{7}
Sr-90/Y-90	1.36×10^{11}	Eu-154	1.87×10^{10}	Sr-90/Y-90	2.05×10^{11}	Eu-154	3.54×10^{10}
Kr-85	6.44×10^{9}	Eu-155	6.59×10^{9}	Kr-85	1.05×10^{9}	Eu-155	1.50×10^{9}
Zr-93	1.30×10^{7}	U-236	5.33×10^{5}	Zr-93	2.07×10^{7}	U-236	3.29×10^{5}
Nb-93m	1.00×10^{7}	U-238	2.68×10^{6}	Nb-93m	1.57×10^{7}	U-238	1.89×10^{6}
Tc-99	6.67×10^{7}	Np-237	8.26×10^{5}	Tc-99	9.04×10^{7}	Np-237	1.49×10^{5}
Ru-106/Rh-106	4.19×10^{8}	Pu-238	3.53×10^{10}	Ru-106/Rh-106	8.52×10^{8}	Pu-238	4.07×10^{10}
Pd-107	1.04×10^{6}	Pu-239	1.09×10^{9}	Pd-107	2.19×10^{6}	Pu-239	1.09×10^{9}
Cd-113m	6.41×10^{7}	Pu-240	2.28×10^{9}	Cd-113m	1.37×10^{7}	Pu-240	2.13×10^{9}
Sb-125	7.11×10^{8}	Pu-241	3.30×10^{11}	Sb-125	1.37×10^{8}	Pu-241	4.07×10^{11}
Te-125m	1.74×10^{8}	Pu-242	3.09×10^{7}	Te-125m	3.34×10^{8}	Pu-242	5.81×10^{7}
I-129	1.87×10^{5}	Am-241	1.18×10^{10}	I-129	3.31×10^{5}	Am-241	1.14×10^{10}
Cs-134	6.96×10^{9}	Am-243	3.22×10^{8}	Cs-134	2.50×10^{9}	Am-243	1.09×10^{8}
Cs-135	5.74×10^{6}	Cm-244	2.21×10^{10}	Cs-135	8.44×10^{6}	Cm-244	3.47×10^{10}
Cs-137	2.99×10^{11}	Cm-245	3.24×10^{6}	Cs-137	5.52×10^{11}	Cm-245	2.40×10^{6}
Ce-144	4.96×10^{7}	Cm-246	1.62×10^{6}	Ce-144	9.48×10^{7}	Cm-246	3.50×10^{6}
Sn-126	3.70×10^{6}			Sn-126	7.15×10^{6}		
Pm-147	1.26×10^{10}			Pm-147	1.70×10^{10}		
Sm-151	5.56×10^{8}			Sm-151	8.48×10^{8}		

The yields of the radionuclides outlined in Table 3 are generally low compared with those from other impurities (Table 2) with the exception of Cs-137 [2].

2 Impurity and isotopes analysis

2.1 Inductively Coupled Plasma, Gas Chromatography

The University of Manchester aims to analysis the impurity inventory of the graphite grades used in the UK reactors and investigate the location of the impurities within the graphite structure. Investigations are currently underway for three British reactors: the British Experimental Pile Zero (BEPO), the Magnox design and AGRs. Quantification of impurities will be determined using Inductively Coupled Plasma, Gas Chromatography-Mass Spectrometer (ICPGC-MS) an example of which is shown in Figure 1.

Figure 1: Example of an ICPGC-MS equipment

These results will then be inputted into the UKAEA FISPACT software [12] (developed from the FISPIN code) to determine the resultant radionuclides which are produced when the impurities found using the ICPGC-MS are exposed to the reactor flux (which will be

simulated using physics codes). The software allows the determination of the relative production pathways for each radionuclide, allowing us to investigate the relative contributions from each of the impurities to that of the final radionuclide inventory. The impurities and isotopes formed within the material from activated impurities may be a verified and characterised using addition techniques such as Autoradiography and X-ray tomography.

2.2 Autoradiography

Autoradiography provides a visual distribution pattern of radiation present in the surface of a sample, depending on isotope energy [13, 14]. Autoradiography can therefore determine β and γ radiation present within nuclear graphite with energy above 0.018MeV. Weak β-emitting isotopes and α isotopes are stopped by the coating on the phosphorous storage film (recording medium). Autoradiography is a qualitative technique used to analyse high energy β and γ isotopes present within a nuclear graphite sample.

The phosphor storage screens comprise of fine crystals of $BaFBr:Eu^{+2}$ in an organic binder. Upon exposure to radiation the Eu^{+2} is excited to the oxidised Eu^{+3} state and the BaFBr is reduced to $BaFBr^{-}$. The phosphor storage screen releases this energy when exposed to light of an appropriate wavelength. Excited electrons fall to the ground state thus releasing energy in the form of blue light. The emitted light passes through a photomultiplier detector which converted to produce an electric current proportional to the activity in the sample.

The advantages of this technique include reduced exposure time compared to traditional autoradiography using X-ray film and increased sensitivity with a linear dynamic range of 1 to 100000 which allows both weak and strong energy isotopes to be analysed simultaneously.

2.3 Autoradiography Analysis at the UoM

A Typhoon 9410 Amersham instrument has been used throughout this study. Sample size, or preferentially diameter is shown to have significant effect on the autoradiography results. Autoradiography analysis of graphite samples thicker than 1cm have proved difficult to analyse with the high energy radionuclide's saturating the film after only a 4 - 6 hours, making comparison between graphite samples that have acquired varying levels of dose or exposure inconclusive.

In total 60 samples where analysed. The sample size was 1mm in diameter and manually cut from using a saw. The autoradiography screen was wiped clean after each use using a light box and a lint free cloth. The samples were placed on the screen in a glove box and left for 20 hours. This length of time was determined as sufficient exposure time without saturating the film due to the activity present in the graphite and will vary for each type of sample being analysed.

Analysis of the film performed using the Amersham (wavelength of 633nm) and a pixel size of 50 microns. The average intensity, standard deviation, variance, minimum and maximum intensity and area are calculated. This allows the background to be deducted from analysis and documents any errors between results.

Autoradiography was carried out on all BEPO samples in order to gain a qualitative assessment of the distribution of radioisotopes within the irradiated BEPO material. Figure 2 shows the average intensity of the samples with increasing sample number s after an exposure time of 20 hours . Sample 1 exhibits the least intensity of the BEPO materials, which corresponds to the least active samples s. there is a non uniform distribution of

radioisotopes which can be noted by the presence of high intensity regions contained within sample 16 this is also a high distribution of activity with both sample 20 and 21 this film is fully saturated and again shows a non uniform disruption of β and γ activity within the sample.

A)

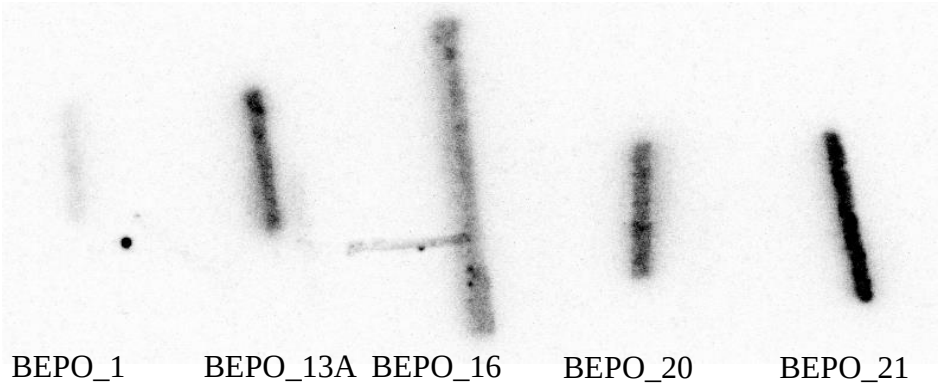

B)

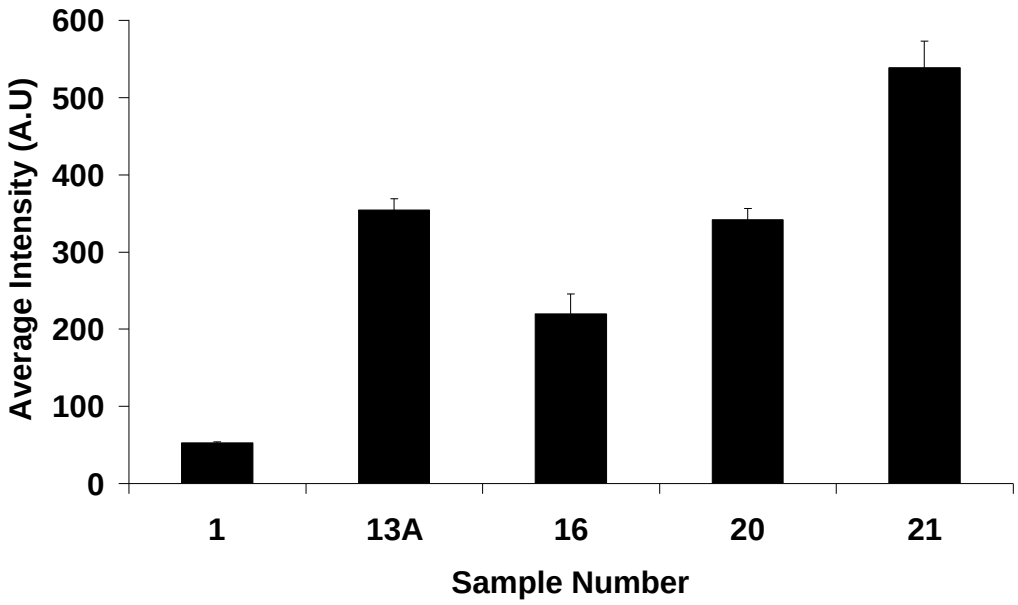

Figure 2: A) Autoradiograph showing increasing greyscale intensities with exposed BEPO samples, B) graph showing the average intensity for BEPO samples.

2.4 X-ray Tomography

Computerised x-ray tomography is a non destructive technique that allows the 3D microstructure of irradiated graphite to be analysed. This technique involves sending an X-ray beam thorough the material and recording the transmitted beam using a charged coupled device camera as shown in Figure 3. The ratio of transmitted to incident photons is related to the integral of the absorption coefficient of the material along the path that the photons made through the material. Using an empirical law, the absorption coefficient can be related to the density, the atomic number and in certain cases, the energy [15-17]. The resulting radiograph is a projection of a volume in a given 2D plane. The method of acquiring a 3D image is to obtain radiographs whilst rotating the sample between 0° and 180°. An algorithm (filtered back-projection) is applied to reconstruct the volume from the 2D radiographs.

This CT data was used to determine porosity and density of the BEPO graphite. The smallest porosity or characteristics that can be identified however are limited to the resolution of the 2D radiographs which is determined by the sample size and CCD camera used.

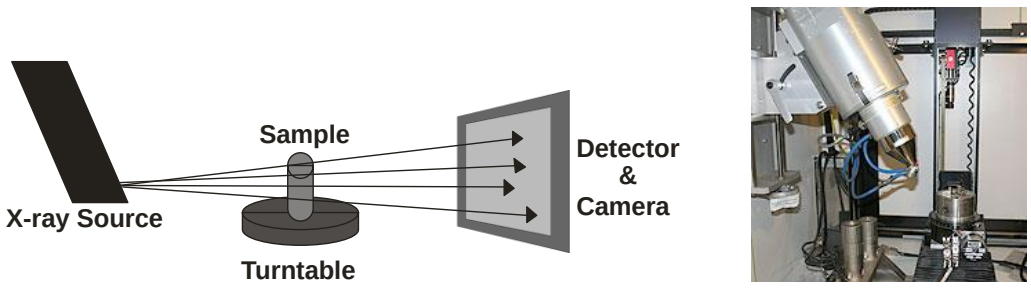

Figure 3. A) Schematic and B) photograph of X-ray tomography scanner;

2.5 X-ray Tomography Analysis at the UoM

Tomography images were collected using the X-TEK HMX CT instrument using the parameters outlined in Table 4. In addition, a rotation of 0.3º with 32 frames and a camera exposure time of 160s were also applied. A voxel size of 21.4 µm was resolved.

Irradiated graphite analysis was performed with the samples contained within a 'harwell can', this ensured that no radioactive graphite dust would contaminate the tomography equipment. No filter was applied during the analysis as the can is made out of aluminium thus acting as a filter. A calibration of the can's thickness versus attenuation using highly orientated pyrolytic graphite (HOPG) as a reference standard inside the can is shown in Figure 4 where intensity shown to exhibit a linear relationship with thickness. The reconstruction of the 2D images was completed using Amira© software and are shown in Figure 5.

Table 4: Tomography experimental parameters

Parameters	Settings
Target	Copper
Filter	None
Detector	Beryllium
Voltage	95 kV
Current	105 µA

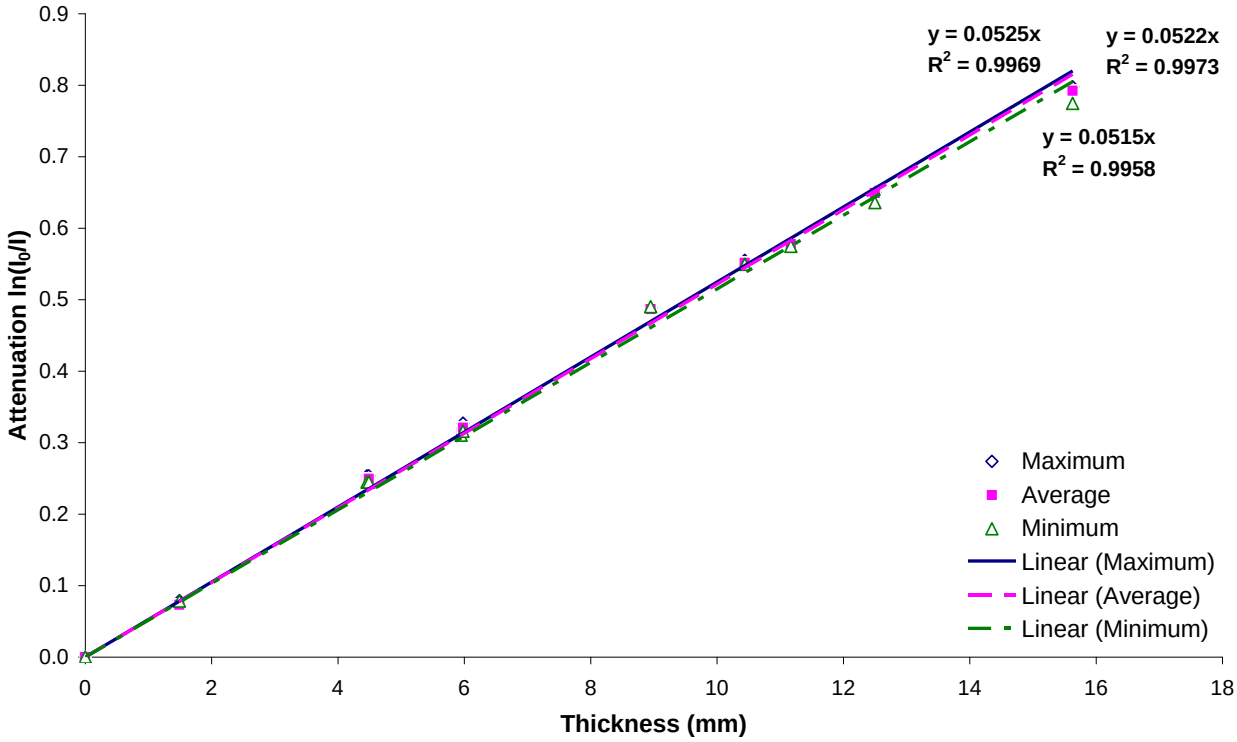

Figure 4: Calibration graph of thickness of HOPG sample inside a harwell can versus the attenuation intensity of the transmitted incident photons that have passed thorough the HOPG sample.

2D slices of BEPO graphite with high attenuation are observed and shown in Figure 5. These spots are of a material with a much higher density and therefore elemental number than that of graphite. The majority of these high attenuation spot are noted to be next to or contained within areas of porosity.

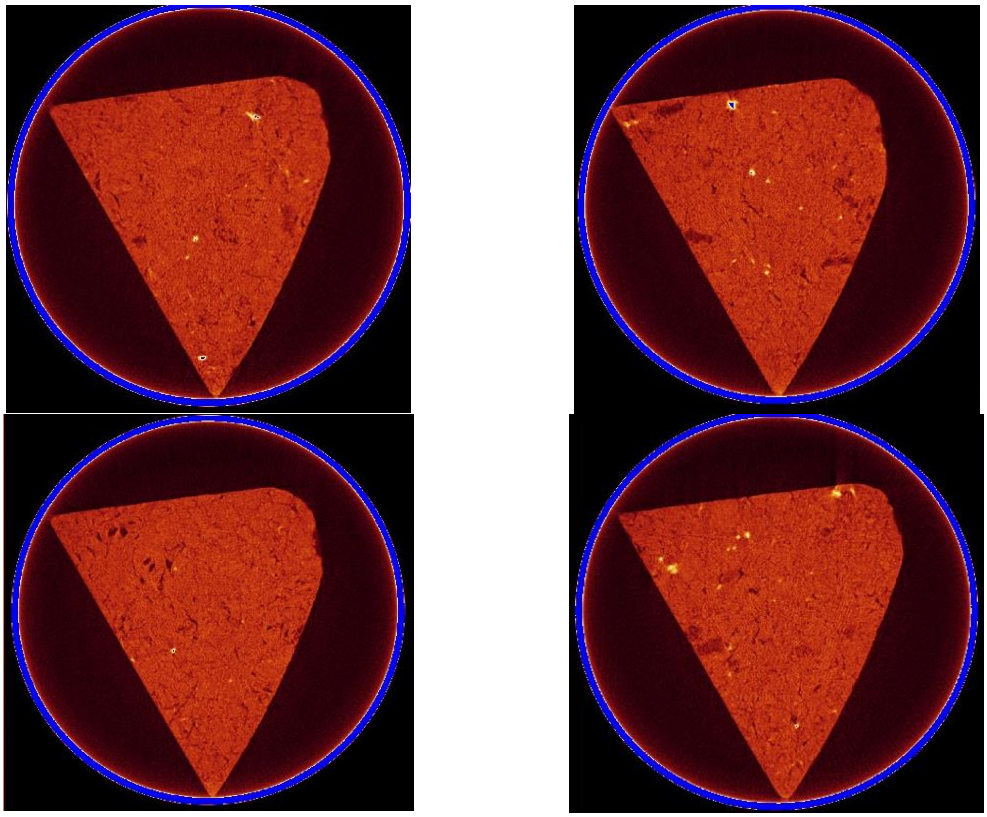

Figure 5: 2D tomography Radiographs of BEPO sample 16 graphite contained within a Harwall can.

3D volume reconstructions of BEPO sample 16 have been processed using Amira© software are shown in Figure 6. The porosity distribution was calculated and is equivalent to 17.2% porosity. The blue regions display the internal porosity and the red is the high attenuation spots. It can be noted the is these high attenuations spots are contained within the porosity and are non uniformly distributed.

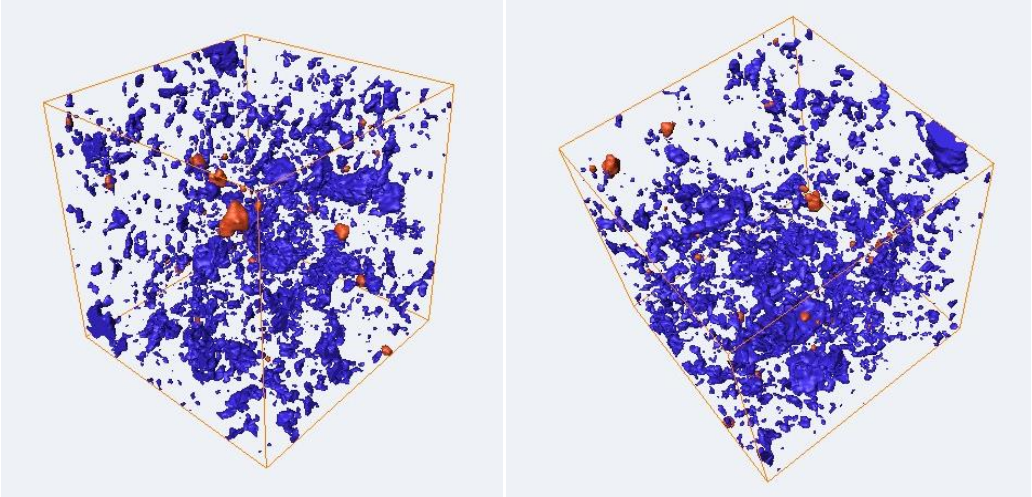

Figure 6: 3D volume reconstructions of BEPO Graphite using Amira© software

3 Summary

This task will build on analysis of data for the various grades of unirradiated and irradiated graphite obtained in WP3 in conjunction with data obtained for the treated graphite in WP4. Mechanistic background of impurity / isotope localisation before and after treatment is required to feed into the treatment options within WP4 and subsequent work packages. A literature review is underway to investigate the mechanistic background of impurity content and removal of irradiated graphite waste. The process involved in predicting the end of life radionuclide inventory has been identified and research is underway in order to apply this to a statistical model for impurity removal. Techniques such as ICPGC-MS, Autoradiography, SEM-EDX and X-ray tomography have also been highlighted for the analysis of impurity and isotopic location within the graphite. These models for the removal of the contaminants will be defined and validated against the data and known inventories and will be developed over the next two years. A fundamental understanding radionuclide origins, location as removal mechanisms, combined with the development of

improved graphite purification methods, may enable the manufacture of new grades of nuclear graphite with lower impurity concentrations being important for both, improved neutronics and waste minimisation.

4 References

1. Nightingale, R.E., *Nuclear Graphite*. 1962, New York: Academic Press.
2. Wickham, A.J. and B.J. Marsden, *Characterisation, Treatment and Conditioning of Radioactive Graphite from Decommissioning of Nuclear Reactors.* IAEA TECDOC-1521,, 2006.
3. White, I.F., et al., *Assessment of Graphite management modesfor graphite form reactor decommissioning*, in *CEC*, E. Commission, Editor. 1984.
4. Fachinger, J., *14C and 3H Thermal Treatment from Merlin Graphite*, in *CARBOWASTE: 2nd Annual steering committee meeting*, A.N. Jones, Editor. 2009: Marcoule, France.
5. FZJ, *CARBOWASTE Treatment and Disposal of Irradiated Graphite and Other Carbonaceous Waste Grant agreement no.: 211333*. 2008.
6. von Lensa, W., *CARBOWASTE: New EURATOM Project on 'Treatment and Disposal of Irradiated Graphite and other Carbonaceous Waste'*, in *Proceedings of the 4th International Topical Meeting on High-Temperature Reactor Technology*, HTR2008, Editor. 2008: Washington D.C., USA.
7. Guiroy, J.J., *Graphite waste incineration in a fluidized bed*, in *Specialists meeting on graphite moderator lifecycle behaviour*, I.A.E. Agency, Editor. 1995, International Atomic Energy Agency: Bath, UK. p. 193-203.

8. Kelly, B.T., *Graphite - The Most Fascinating Nuclear Material.* Carbon, 1982. **20**(1): p. 3-11.

9. Hou, X., *Rapid analysis of 14C and 3H in graphite and concrete for decommissioning of nuclear reactor.* Applied Radiation and Isotopes, 2005. **62**(6): p. 871-882.

10. Wampler, W.R., et al., *Trapping of deuterium at damage in graphite.* Journal of Nuclear Materials, 1990. **176-77**: p. 983-986.

11. Hou, X., L.F. Ostergaard, and S.P. Nielsen, *Determination of 36Cl in Nuclear Waste from Reactor Decommissioning.* Anal. Chem., 2007. **79**(8): p. 3126-3134.

12. Forrest, R.A. and J. Kopecky, *The activation system EASY-2007.* Journal of Nuclear Materials.

13. Bauer, E., *STUDIES OF THE INITIAL PHASES OF OXIDATION OF NUCLEAR GRAPHITE IN AIR AT TEMPERATURES BETWEEN 420 AND 650 C.* Journal de Chimie Physique (France) Merged with Rev. Gen. Colloides to form J. Chim. Phys. Rev. Gen. Colloides; Vol: 58, 1961: p. Pages: 47-52.

14. *Introduction to Autoradiography.* 1998.

15. Berre, C., et al., *Numerical modelling of the effects of porosity changes on the mechanical properties of nuclear graphite.* Journal of Nuclear Materials, 2006. **352**(1-3): p. 1-5.

16. Babout, L., et al., *The effect of thermal oxidation on polycrystalline graphite studied by X-ray tomography.* Carbon, 2005. **43**(4): p. 765-774.

17. Babout, L., et al., *Three-dimensional characterization and thermal property modelling of thermally oxidized nuclear graphite.* Acta Materialia, 2008. **56**(16): p. 4242-4254.